Engineering and Technology Journal
Journal homepage: https://etj.uotechnology.edu.iq

Effect of Ag-PTFE nanocomposite coating on wettability and antimicrobial activity of orthodontic wires

Mahmood S. Naser [a,b*], **Emad Al-Hassani** [b], **Fatima Al-Hassani** [b]

[a] Department of Materials Engineering, Faculty of Engineering, University of Kufa, Iraq.
[b] College of Materials Engineering, University of Technology, Alsinaa street, 10066 Baghdad, Iraq.
*Corresponding author Email: mahmoods.alammar@uokufa.edu.iq

HIGHLIGHTS

- Ag-PTFE nanocomposite coating was successfully prepared.
- The Ag-PTFE coating layer was characterized in detail.
- The coated stainless-steel wire changed from hydrophilic to hydrophobic.
- Microbial growth was strongly inhibited on the coated stainless-steel wire.

Keywords:

Radio frequency
Archwires
Ion release
Wettability
Antibacterial

ABSTRACT

This study investigates the effect of Ag–PTFE nanocomposite coatings, prepared by radio frequency (RF) sputtering, on the surface and antimicrobial properties of orthodontic stainless steel archwires (SSW). The novelty lies in combining silver (Ag) and polytetrafluoroethylene (PTFE) nanoparticles into one coating, which has not been widely applied to orthodontics. The motivation is the need to reduce microbial adhesion and biofilm on archwires, which contribute to enamel demineralization, gingival disease, and infections. The problem addressed is the lack of coatings that can simultaneously provide enhanced surface properties, facilitate controlled silver ion release, and deliver durable antibacterial performance. Unlike literature that mainly studied Ag or polymer coatings separately, this work fills the gap by varying Ag and PTFE weight percentages and assessing their combined effects on wettability, roughness, ion release, and antimicrobial activity. Austenitic 316L stainless steel archwires (0.4 mm in diameter and 160 mm in length) were coated using Ag and PTFE nanopowders (30 nm). The coated SSW was characterized using field emission scanning electron microscopy (FESEM), X-ray diffraction (XRD), and contact angle measurements, while silver ion release was analyzed by atomic absorption spectroscopy. Antimicrobial efficacy was tested against Streptococcus mutans and Staphylococcus aureus. The results showed uniform coatings with distinct hydrophobic behavior and antibacterial activity. Increasing Ag content enhanced silver ion release and inhibition zones, while higher PTFE content increased hydrophobicity, reducing bacterial adhesion. These findings highlight Ag–PTFE coatings as a synergistic strategy to improve surface properties and suppress microbial colonization, suggesting potential benefits in preventing caries and periodontal complications.

1. Introduction

Fixed appliances are recognized for their role in promoting the accumulation and retention of plaque. Individuals undergoing orthodontic treatment who exhibit inadequate oral hygiene are likely to present with saliva that has a higher acidity level. As a result, these patients may experience an increased release of nickel ions, which can trigger allergic reactions [1]. White spot lesions or carious demineralization often occur as unintended consequences of orthodontic treatment. Numerous studies have found that orthodontic procedures can significantly elevate the chance of white spot lesions formation [2,3]. Findings from various studies indicate that white spot lesions can advance swiftly during the initial weeks of orthodontic treatment [4]. Furthermore, the occurrence of demineralization surrounding fixed orthodontic appliances exceeds the usual rate of carious lesion formation, as demonstrated by the initiation of enamel demineralization predominantly occurring within the initial six months of commencing orthodontic treatment. The occurrence could reach up to 46% within a year following the bonding of fixed appliances [5].

http://doi.org/10.30684/etj.2025.163995.2004
Received 13 August 2025; Received in revised form 05 September 2025; Accepted 06 September 2025; Available online 02 October 2025
2412-0758/University of Technology-Iraq, Baghdad, Iraq

Moreover, the expansion of the oral microbial community, along with notable changes in subgingival microbiomes and an elevated level of bacterial resistance linked to fixed appliance intervention, increased the occurrence of localized gingivitis/mild periodontitis [6]. From the initiation of orthodontic treatment, it is widely acknowledged that maintaining excellent oral hygiene serves as a crucial preventive strategy that aids in the health and recovery of patients' gingival and periodontal tissues after treatment. Furthermore, the prevention of lesions and cavities can be achieved through the removal of bacterial plaques utilizing mechanical techniques, mouth rinses, and fluoride treatments [7]. Nonetheless, patient adherence is essential for the effectiveness of this preventive approach [8]. The installation of a fixed orthodontic appliance often leads to a notable deterioration in oral health and hygiene among patients. This decline is generally linked to the discomfort experienced during the adjustment of teeth to their new positions, as well as the challenges in maintaining proper oral hygiene due to the presence of various irregular surfaces. Consequently, multiple approaches have been developed to enhance implant surfaces with antibacterial properties, aiming to inhibit or slow bacterial contamination [10,11].

Silver (Ag)-based coatings have generated significant attention due to the broad-spectrum antibacterial properties of silver and its minimal risk of fostering bacterial resistance [12,13]. Silver nanoparticles (Ag NPs) have been utilized in dentistry to develop antimicrobial compounds, aiming to enhance the quality of dental products and improve treatment outcomes [14]. These materials can be incorporated into various dental care products, such as titanium coatings for dental implants, gingival membranes for aided tissue regeneration, orthodontic adhesives, and composite and acrylic resins for direct restoration [15,16].

Due to its extensive specific surface area, Ag NPs exhibited notable inhibitory and antimicrobial effectiveness against a broad range of pathogens, including bacteria, fungal species, and viruses, while preventing the emergence of microbial resistance. Furthermore, it has been demonstrated that silver ions (Ag^+) can effectively impede the formation of biofilms [17]. Surface proteins represent the most sensitive sites to Ag^+, and any modifications to these proteins lead to bacterial disruption through significant structural and metabolic damage. The release of Ag^+ can influence the permeability of membranes, leading to the release of cytoplasm and possibly resulting in cell death [18]. The antibacterial properties of Ag NPs are coupled with the protective and durable properties of polytetrafluoroethylene (PTFE) to create a powerful combination. The PTFE enhances the stability and longevity of Ag NPs, preventing them from leaching or agglomerating. PTFE demonstrates remarkable chemical stability, is non-toxic to humans, and shows high resistance to both heat and chemicals. It also exhibits outstanding hydrophobic characteristics, along with superior anti-sticking properties, and possesses an exceptionally low coefficient of friction. Consequently, PTFE finds extensive application in the medical field and is particularly well-suited for orthodontic devices, such as wires [19-21].

Among the techniques employed for creating metal-polymer nanocomposites, radiofrequency magnetron sputtering (RF) has emerged as a prevalent method for thin film deposition (from a few nanometers to several micrometers, depending on the operational parameters such as deposition time, beam energy, etc.), utilizing solid targets as the starting material. The physical processes involved in removing atoms from organic and inorganic targets and subsequently depositing them onto a substrate. This process has numerous advantages over other processes, including a rapid deposition rate, outstanding uniformity across relatively large surfaces, and remarkable conformality over substrates with varying topographies [22,23]. This study presents the advancement of antimicrobial (Ag–PTFE) nanocomposite thin films produced through RF sputtering techniques. This study details the morphological and compositional characteristics of Ag–PTFE nanocomposite biomaterial produced through this method. The innovative application of nanoparticles, specifically the combination of PTFE with Ag, represents a significant advancement in coating archwires.

2. Materials and methods

2.1 Materials

The main raw materials used in this study are shown in Table 1.

Table 1: Description of the main materials utilized in this study

NO.	Material	Specifications
1	316L stainless steel upper archwires (SSW)	Diameter: 0.4 mm Length: 160 mm Company: Dentaurum, Germany.
2	Silver nano powder (Ag)	Size: 30 nm Purity: > 99.95 % Density: 0.5 g/cm^3 Company: Yujiang Chemical, China.
3	Polytetrafluoroethylene nano powder (PTFE)	Size: 30 nm Purity: > 99.95 % Density: 2.2 g/cm^3 Company: Yujiang Chemical, China.

2.2 Methods

2.2.1 Archwires preparation for RF sputtering process

SSW were ultrasonically cleaned in ethanol and then in distilled water for 10 minutes each. Archwires were then dried in a drying furnace (HQHAOTWU, China) at 50 ℃ for 10 minutes and sterilized using an ultraviolet (UV) light cabinet (Analytic, Germany) for 30 minutes to remove accumulated contaminants (Figure 1).

Figure 1: Procedures for archwires preparation

2.2.2 Target Preparation for RF sputtering process

The RF targets were made from three different weight percentages (wt.%) of Ag and PTFE nano powders, as illustrated in Table 2. These percentages were mixed in a tank mixer (MTI, USA) for 2 hours at 100 rpm and then pressed in a mold under 500 MPa pressure and held for 5 minutes by using a hydraulic press (Mega, PRDE (30T/50T), Spain) to produce a compact with dimensions of 50 mm diameter and 4 mm thickness.

Table 2: Different weight percentages of RF target

Group Symbol	Ag Powder (wt. %)	PTFE Powder (wt. %)
A	80	20
B	70	30
C	60	40

2.2.3 RF sputtering process

The three different RF targets (A, B, and C) were mounted one by one on the cathode, and the SSWs were placed on the anode, with their sides facing the target holder using an RF sputtering system (Barez Afarin Industry, Iran). The RF chamber was evacuated to a specified pressure, and then argon gas (99.99% purity) was introduced into the chamber. The substrate holder was maintained rotating during the sputtering process. The Ag–PTFE film was sputtered for 30 minutes, and all archwires were prepared at ambient temperature. The sputtering parameters are listed in Table 3, and the RF diagram and device are shown in Figure 2 (a and b) respectively.

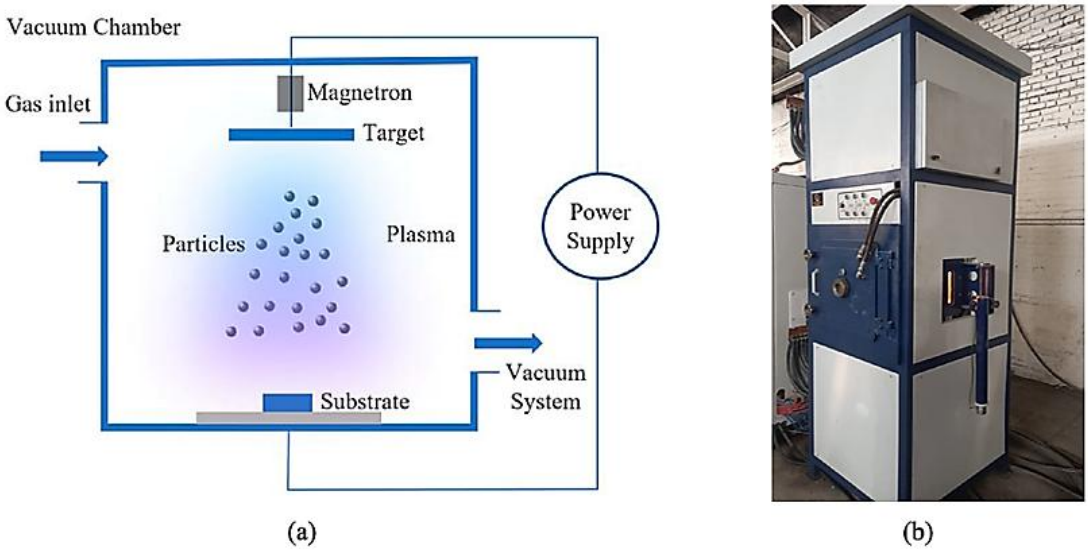

Figure 2: a) Diagram of the RF sputtering process [24], and b) RF sputtering system

Table 3: RF sputtering parameters used in this study

RF Sputtering variables	Value
Power	60 W
Evacuation pressure	6×10^{-4} Pa
Target-to-substrate distance	50 mm
Gas flow rate (Argon)	20 mL/min
Sputtering time	30 min
Target composition	Ag–PTFE
Substrate holder rotating speed	20 RPM

2.2.4 Artificial saliva preparation

The artificial saliva was obtained by dissolving the chemical components listed in Table 4 in 1,000 mL of distilled water using a magnetic stirrer. Following thorough dissolution in water, the mixture underwent filtration through filter paper with 0.5 µm pores to eliminate any impurities, ensuring the saliva achieved maximum purity. Ultimately, sodium hydroxide (NaOH) and lactic acid were incorporated to fine-tune the pH level of the artificial saliva to 6.7 ± 0.1 [25].

Table 4: Artificial saliva compounds [26]

Chemical Product	Composition (g/L)
K_2HPO_4	0.22
KCl	1.19
KSCN	0.29
Na_2HPO_4	0.26
NaCl	0.69
$NaHCO_3$	1.49
Urea	1.49

2.2.5 Statistical analysis

A descriptive statistic was used in this study for all data of contact angle testing, which were organized, categorized, and transferred into a computerized database structure using the SPSS program, including Minimum (Min), Maximum (Max), Mean (M), and Standard deviation (SD). and data were screened for normal distribution using the Shapiro-Wilk. These tests were used to either accept or reject the statistical hypothesis, establishing a 95% confidence interval. Moreover, one-way ANOVA and Tukey HSD post hoc multiple-comparison tests were used to test whether there were significant differences between the three different weights.% coated SSW imposing an interval of confidence of 95%. The significance level was considered significant when the P-value was less than 0.05.

3. Characterization of coating layer

3.1 X-Ray Diffraction (XRD)

X-ray diffraction was performed to determine the presence of phases and crystallographic properties of the raw materials, the coated and uncoated SSW, using an X-ray diffractometer (Chongqing Drawell, China) with a nickel filter and a copper generator. The speed of scanning was adjusted to 6 deg.min^{-1}, and the diffraction angle ($2\theta^o$) range was (10 °- 80 °). The resulting peaks were compared with the standard peaks for each material using the Joint Committee on Powder Diffraction Standards (JCPDS) cards. The crystallite size (particle size) of Ag and PTFE was determined using the Scherrer formula to ensure the nanosize of the powders used. The particle size (D) can be estimated from Equation 1 [27]:

$$D = 0.9\lambda \,/\, FWHM\ Cos\theta \quad (1)$$

where: D: The size of the crystallites measured in nanometers. λ: represents the wavelength associated with Cu Kα, measured at 0.15406 nm. FWHM: The full width at half maximum of the diffraction peak is measured in radians. θ: The semi-angle of diffraction or Bragg angle (degree).

Finally, the quantitative phase contents in polycrystalline materials were calculated through an iterative least-squares fitting process using Rietveld refinement [28] for the diffraction data by the X'Pert HighScore Plus program.

3.2 Field emission scanning electron microscopy (FESEM)

The nanoparticles' morphology and distribution, as well as the coating layer thickness, were examined by field-emission scanning electron microscopy (FESEM) (TESCAN MIRA3, France). The elemental composition and mapping of the SSW were examined utilizing energy dispersive X-ray spectroscopy (EDX) in conjunction with FESEM.

3.3 Ion release assessment

To evaluate the amount of Ag^+ ions released from the coating layer, the coated SSW segments were immersed in 5 mL of artificial saliva solution in test tubes. These tubes were closed tightly and incubated at 37 °C for 4 weeks. The total Ag^+

concentrations in the saliva solution after 1, 5, 10, 15, 20, 25, and 30 days were quantified using an atomic absorption spectrophotometer (Shimadzu AA7000, Japan).

3.4 Wettability evaluation

The assessment of wettability or hydrophobicity for both coated and uncoated samples was conducted through the application of a static drop of distilled water, and the liquid and solid contact angles were measured with an optical contact angle meter (SL200KS, China) by the sessile drop technique. The methodology consisted of applying one µL of distilled water onto the surface of the sample and recording the contact angle of the water over a duration of 10 seconds, repeated three times for each sample. The average value of the measured contact angles was then taken.

3.5 Antibacterial assay

The antibacterial activities of the coated SSWs were demonstrated against the bacterial strains Streptococcus mutans (S. mutans) and Staphylococcus aureus (S. aureus). The agar well diffusion method was employed to examine the antimicrobial properties of both uncoated and coated SSW. The prepared cultures were spread on petri dishes, and then the samples were placed in the incubator. After incubation for 24 h at 37 °C, the inhibition zone size was calculated using a ruler.

4. Results and discussion

4.1 X-Ray Diffraction

Figure 3 illustrates the patterns obtained from X-ray diffraction analysis of the raw materials and coated SSW, it can be seen that the standard peaks of stainless steel 316L in Figure 3a reference to JCPDS card No. 33-0397 for the primary austenite (γ-Fe) cubic phase with their main plane (111), (200) and (220) were present and this confirms that the primary austenitic phase is present and of high quality [29]. The diffraction peaks of Ag nano powder in Figure 3b, this diffraction pattern revealed sharp and well-defined peak intensities at 2θ values of 37.6º, 44.0º, 64.4º and 77.3º, which corresponds to the (111), (200), (220) and (311) planes without any noticeable amorphous background, indicating a high degree of crystallinity, estimated to be nearly 100%. Furthermore, the observed peaks correspond exclusively to the face-centered cubic (FCC) structure of metallic silver, with no evidence of secondary phases such as silver oxides. All the peaks corresponded accurately with the standard JCPDS card No. 04-0783 for cubic Ag NPs [30]. The crystal size of the Ag powder was estimated by applying the Scherrer equation, as shown in Table 5, and is 31.204 nm, which falls within the nanoscale range (1~100 nm) [31]. This is in agreement with AFM analysis as shown in Figure 4. Therefore, based on Rietveld refinement, it can be concluded that the sample is composed of a single crystalline phase (FCC-Ag) with a purity close to 100% and exhibits excellent structural order.

Table 5: Particle size of Ag nano powder

2 Theta (º)	FWHM (rad)	Intensity (%)	Size (nm)
38.3022	0.246	100	34.224
44.5023	0.246	30.07	34.926
64.5991	0.3444	19.9	27.337
77.4884	0.36	19.29	28.331
	Average		31.204

On the other hand, the PTFE Pattern illustrated in Figure 3c exhibits distinct broad peaks centered around 18–20° (2θ), indicating a semi-crystalline nature typical of PTFE, and every peak corresponded with the reference JCPDS card No. 00-045-1594 for PTFE [32]. In PTFE nano powders, the peaks may be slightly broadened or shifted compared to those of bulk PTFE due to size effects and an increased surface area [33]. Rietveld analysis confirmed the presence of a single crystalline phase corresponding to hexagonal PTFE, and the degree of crystallinity was estimated to be approximately 82.5%, signifying a dominant crystalline fraction with minor amorphous content. Furthermore, the mean crystallite size was determined employing the Scherrer equation, utilizing data from various peaks (Table 6), yielding a value of approximately 28.722 nm, indicative of nanoscale domain structures.

Finally, the coated Ag–PTFE SSW (Figure 3d) exhibits diffraction peaks corresponding to a thin, fully covered layer of Ag–PTFE, with the presence of the main peak of stainless steel 316L indicating successful sputtering of Ag–PTFE on the SSW.

Table 6: Particle size of PTFE nano powder

2 Theta (º)	FWHM (rad)	Intensity (%)	Size (nm)
18.6253	0.246	66	32.832
20.112	0.246	100	32.765
20.9553	0.3936	65.55	20.571
	Average		28.722

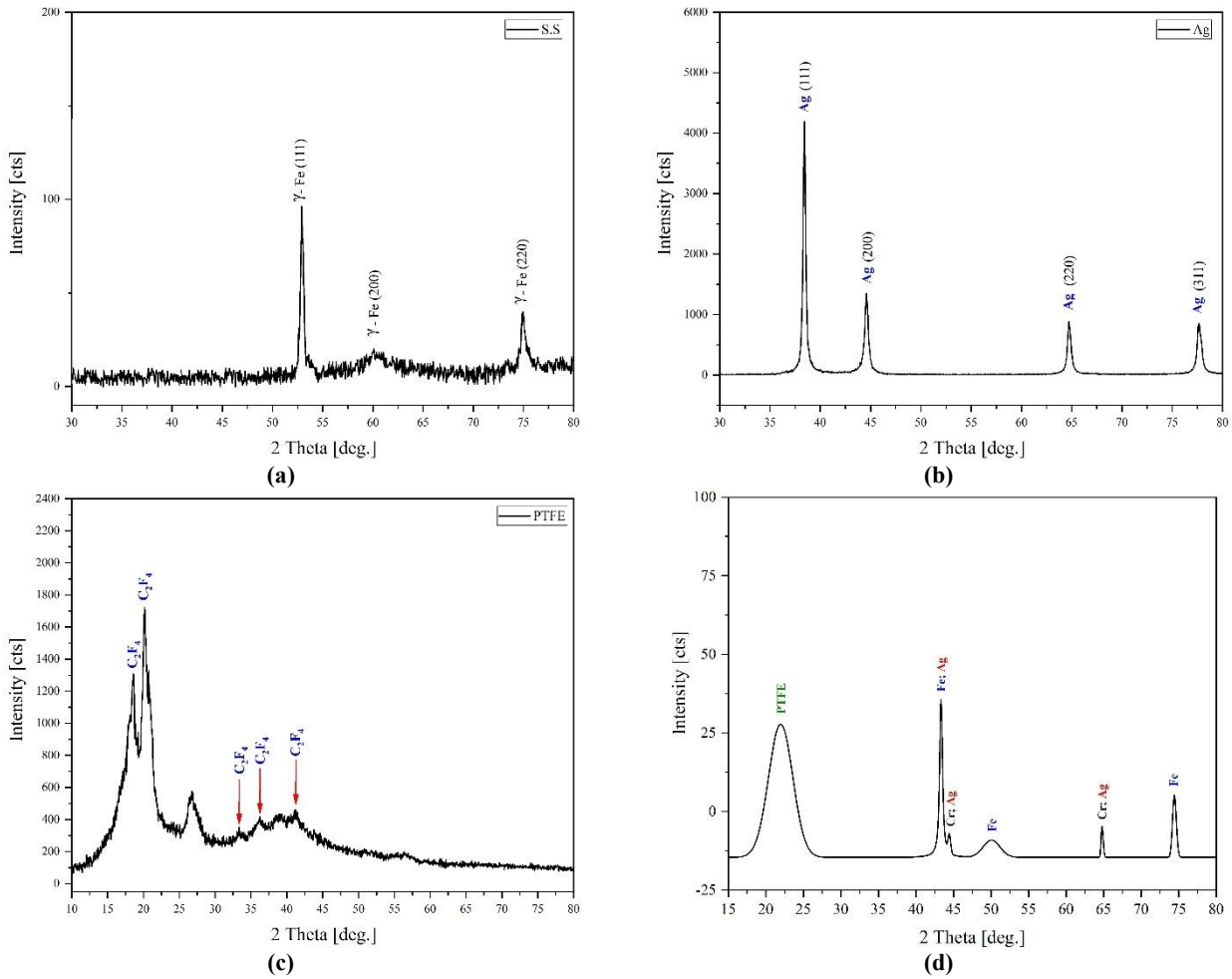

Figure 3: XRD pattern of a) uncoated SSW, b) Ag nano powder, c) PTFE nano powder, and d) Ag–PTFE coated SSW

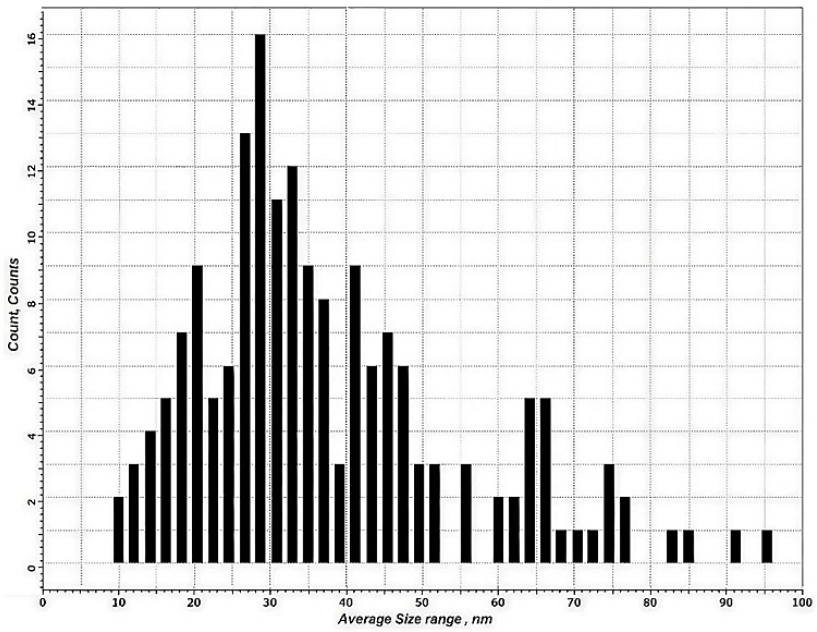

Figure 4: Particle size distribution from AFM of Ag nano powder

4.2 Field emission scanning electron microscopy (FESEM)

The FESEM images of the coated and uncoated SSW at various magnifications (35X, 250X, and 10KX) are shown in Figure 5 (a–f). It indicated a clear difference in the surface morphology between the uncoated control archwire segment and the Ag-PTFE-coated one. The images of the Ag–PTFE NPs-coated SSW segments showed that the nanoparticles had a spherical shape with a homogeneous distribution and no agglomerations.

The EDX results (Figure 6) identified the following elements: Elements of iron (Fe), carbon (C) chromium (Cr) and nickel (Ni) from the substrate as well as silver (Ag), fluorine (F), oxygen (O), and carbon (C) from the sputtered layer demonstrate that the RF sputtering method creates a thin coating (436.78 nm thickness) of Ag–PTFE NPs as shown in Figure 7, which the EDX electrons can penetrate. The decrease in important elements, such as iron (Fe), in the SSW indicates that the Ag–PTFE coating fully covers the substrate. The carbon element detected in the substrate layer utilized for the production of 316L stainless steel is present in minimal quantities, suggesting that the majority of the element is likely derived from the sputtered layer. Fluorine was employed as the standard for detecting the presence of PTFE to mitigate possible inaccuracies. The EDX mapping in Figure 8 (a–c) illustrates the distributions of Ag and F within the coating layer. We notice that the distribution of Ag NPs is higher in sample A, in contrast to the distribution of PTFE particles, which is lower. The distribution of Ag particles begins to decrease in sample B, until it reaches sample D, where it is reversed in the PTFE particles. This is consistent with what we mentioned previously in preparing the samples referred to in Table 2. Additionally, it can be observed that all the particles were distributed regularly and homogeneously, free from agglomeration. These findings indicate that the Ag–PTFE layer has been effectively plated using the RF sputtering technique.

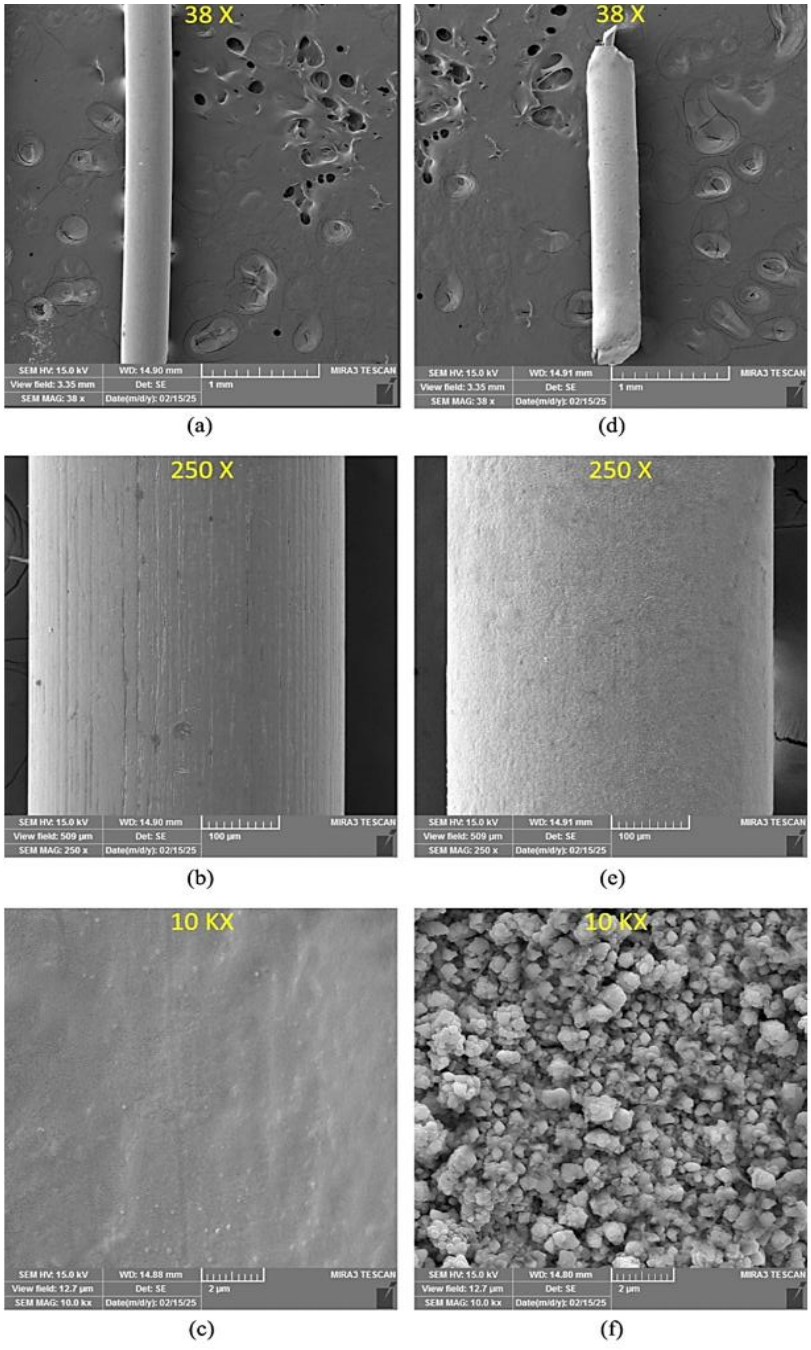

Figure 5: FESEM images of the SSW at different magnification powers for the uncoated (a, b, c) and Ag–PTFE coated SSW (d, e, f) at 30 min

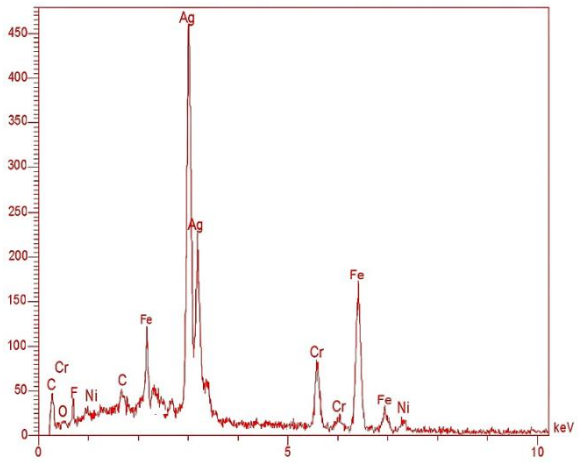

Figure 6: EDX spectroscopy charts for Ag–PTFE-coated SSW

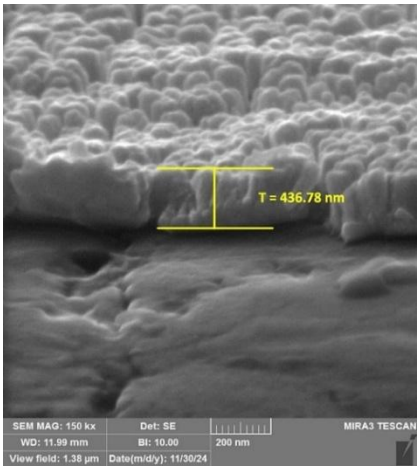

Figure 7: Cross-section microstructure of the Ag–PTFE coating layer after sputtering time 30 min, at 150 KX

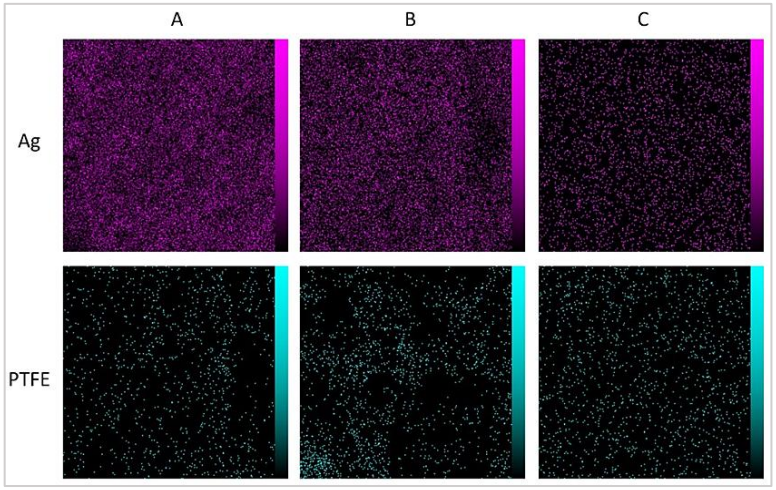

Figure 8: EDX mapping of the FESEM sample coated at 30 min with different weight percentages of Ag and PTFE (A, B, and C)

4.3 Ion release

Previous research indicates that the antibacterial efficacy of nanosilver relies on the release of silver ions and direct interaction with bacteria [34,35]. Research indicates that materials with increased nanosilver loading discharge more Ag^+ and demonstrate a more pronounced inhibitory action [36]. Figure 9 illustrates the release of silver ions (Ag^+) from the Ag–PTFE–coated SSW as a function of immersion duration, extending to 30 days for sample A.

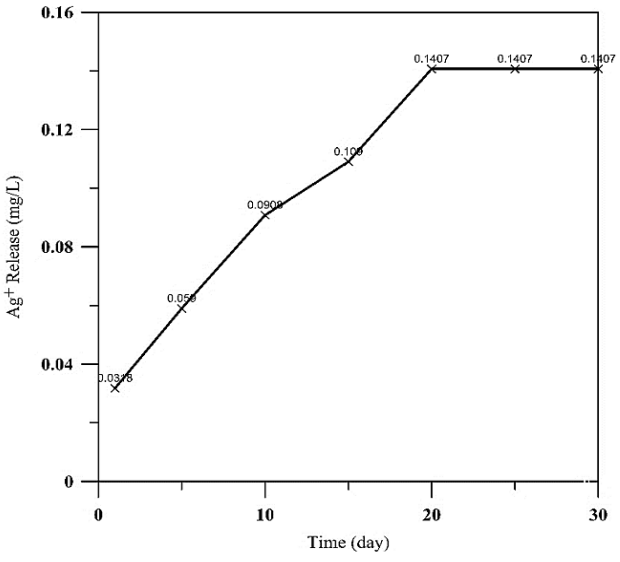

Figure 9: Silver ion (Ag^+) released (mg/L) from the Ag–PTFE coating in 5 mL of artificial saliva

Initially, minimal quantities of Ag^+ were discharged on the first day. Subsequently, the quantities of released Ag^+ progressively increased, and over time, the release rates converged, becoming a relatively stable value of approximately 0.1407 mg/L after 20 days. The incremental rise in Ag^+ release demonstrates that the surface-exposed nanoparticles engage with saliva and are selectively solvated, resulting in a comparatively elevated concentration being released. A further explanation could be that smaller Ag NPs on the substrate exhibit a higher dissolution rate compared to their larger counterparts. The development of Ag clusters impeded the discharge of Ag^+ after 20 days [37]. Previous research indicates that Ag NPs can release silver ions that are capable of eliminating targeted bacterial cells [38]. It was shown that although nanosilver ions released from nanosilver-coated orthodontic wires diminish over extended orthodontic therapy, the antibacterial activity persists through contact inhibition [39].

4.4 Wettability

The statistical results of the contact angle, including the Min, Max, M, SD, and Shapiro-Wilk test values, are shown in Table 7. All the values of the contact angle (CA) were expressed in degrees (°). The water contact angle analysis revealed a gradual increase as the PTFE wt.% increased (Figure 10), with a mean contact angle (CA) of 74.395° for the uncoated SSW. The coated Ag–PTFE layer showed a noticeable influence on the hydrophobic property of sample A. However, the surface of the coated SSW became hydrophobic in sample C, with a contact angle of 135.341° as a result of the higher PTFE content in this sample (40%), consistent with a lower effective solid surface energy on the exposed surface. Consequently, more PTFE at the outermost layer increases the density of fluorinated groups ($–CF_2/CF_3$) presented to the liquid, reducing γ_{SL} (solid–liquid interfacial tension) and raising the apparent contact angle, and this creates a smoother chemically hydrophobic outer layer [40, 41]. According to the Shapiro-Wilk test, the P-value for all samples was more than 0.05, indicating that there is no substantial evidence that the distribution deviates from the normal distribution at the 5% significance level.

Table 7: Statistical description of Contact angle for the bare and Ag–PTFE–coated SSW

Sample Symbol	Sample Condition	N	Min	Max	Mean	SD	Shapiro-Wilk test P-value
SS	Bare SSW	5	72.505	76.764	74.395	1.725	0.785
A	Coated SSW	5	90.836	93.372	92.137	1.066	0.661
B	Coated SSW	5	120.124	126.689	123.394	2.416	0.973
C	Coated SSW	5	131.648	140.438	135.341	3.585	0.617

Figure 10: Contact angle measurements for the uncoated SSW and Ag–PTFE coated SSW at different weight percentages of PTFE

A one-way ANOVA demonstrated a highly significant effect of different weight percentages on the contact angle of SSW ($p = 4.08 \times 10^{-7}$ and effect size $\eta^2 = 0.992$). Post-hoc Tukey's HSD tests showed that all groups differed significantly from each other. Specifically, the mean contact angle increased progressively with increasing PTFE wt.%: bare SSW (74.40° ± 1.73), group A (92.14° ± 1.07), group B (123.39° ± 2.42), and group C (135.34° ± 3.59). The 95% confidence intervals (CI) in Table 8 for all pairwise comparisons did not cross zero, confirming that the observed differences between groups are statistically robust.

Moreover, the relatively narrow confidence ranges (e.g., SS vs A: –20.75 to –14.73) indicate a high level of precision in the estimated mean differences, consistent with the very large effect size ($\eta^2 = 0.992$).

Table 8: Pairwise Comparisons of Contact Angle (Tukey HSD, 95% CI)

Comparison	p-value	95% CI (Lower, Upper)	Significance
SS vs A	<0.001	[-20.75, -14.73]	Significant
SS vs B	<0.001	[-52.00, -45.97]	Significant
SS vs C	<0.001	[-63.96, -57.93]	Significant
A vs B	<0.001	[-34.27, -28.24]	Significant
A vs C	<0.001	[-46.23, -40.20]	Significant
B vs C	0.002	[-14.96, -8.93]	Significant

4.5 Antimicrobial assessment

The antimicrobial activity was observed by the formation of a clear inhibition zone around each coated SSW for both examined microbes. The inhibition zones were observed for both S. mutans and S. aureus microbial species (Figure 11 (a and b)), respetively. The size of inhibition zones for all studied types of microorganisms is shown in Table 9.

As can be seen in Figure 11, there are inhibition zones around the different coated SSW for the two kinds of microbe compared to the uncoated SSW, as a result of the release of a high concentration of compounds on the bacterial cell wall, which resulted in the degradation of the cell membrane of the bacteria, thereby inhibiting bacterial growth [42]. Different sizes of inhibition zones were noticed in Table 9, where sample A had the largest inhibition zone (10.2 mm and 12.1 mm) in both S. mutans and S. aureus respectively compared with samples B and C, due to the higher wt.% of Ag (80%) in sample A and consequently a higher amount of Ag^+ release (0.0318 mg/L) after 1 day of incubation period. This aspect can contribute to decreasing biofilm adhesion and colonization and enhance biocompatibility [43]. On the other hand, the uncoated SSW was unable to inhibit bacterial growth and exhibited bacterial adhesion in S. mutans and S. aureus, respectively. A coupled trend in our data, as the PTFE wt.% increases from 20 to 40, the static water contact angle rises from 92.137° to 135.341°, confirming enhanced hydrophobicity. Over the same composition window, the antibacterial reduction against S. mutans and S. aureus decreases from 10.2 mm to 7.2 mm and from 12.1 mm to 9.8 mm, respectively, consistent with diminished Ag wt.% (confirmed by mapping) and a thicker, less permeable PTFE barrier that limits Ag^+ release. Conversely, Ag-rich coatings show higher killing rates but reduced contact angles (more wetting), likely due to higher surface energy and increased polar sites. The antimicrobial results of the present study are promising in eliminating these serious medical pathogens, as it is clear that the Ag–PTFE layer exhibits good antimicrobial activity.

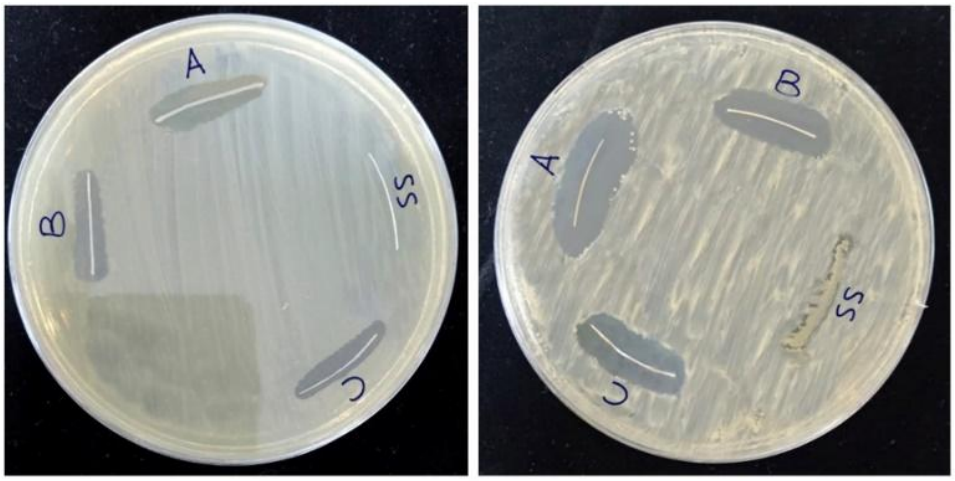

Figure 11: Antimicrobial assessment for the uncoated and coated SSW at different weight percentages of PTFE for a) S. mutans and b) S. aureus

Table 9: Inhibition zones of different coated SSW in different microbial petri dishes

Sample	Inhibition Zone Size (mm)	Microbial Species
SS	No inhibition zone	S. mutans
A	10.2	
B	9.3	
C	7.2	
SS	Bacterial adhesion	S. aureus
A	12.1	
B	11	
C	9.8	

5. Conclusion

In this research, SSWs were successfully nanocomposite coated with Ag–PTFE at different wt.% of Ag and PTFE. The results revealed a uniform and regular thin silver layer covering the wire surface, with no agglomeration observed in the microscopic structure at the nanoscale. The coated SSW exhibited varying degrees of hydrophobic properties, making it inconsistent with liquids and thus less likely to adhere to bacteria. Silver ions also dissolved appropriately, forming a protective layer on the wire that inhibited and killed both types of bacteria. Improving hydrophobicity by increasing PTFE can reduce antibacterial action by shielding silver sites, while higher Ag enhances antibacterial activity but lowers the contact angle. An optimal balance is achieved at intermediate compositions, where surface design allows both properties to meet the minimum required thresholds for the intended application.

Author contributions

Conceptualization, **M. Naser**, **E. Al-Hassani**, and **F. Al-Hassani**; data curation, **M. Naser**; formal analysis, **M. Naser**; investigation, **E. Al-Hassani**; methodology, **F. Al-Hassani**; project administration, **E. Al-Hassani**; resources, **E. Al-Hassani**; software, **M. Naser**; supervision, **E. Al-Hassani**; validation, **M. Naser**, **E. Al-Hassani**, and **F. Al-Hassani**; visualization, **F. Al-Hassani**; writing—original draft preparation, **M. Naser**; writing—review and editing, **M. Naser**. All authors have read and agreed to the published version of the manuscript.

Funding

This research did not receive specific funding from any public, commercial, or non-profit agency.

Data availability statement

Upon reasonable request, the corresponding author will provide the datasets created and examined during the current work.

Conflicts of interest

There are no conflicts of interest, according to the authors.

References

[1] Y. C. Abdulkader, A. F. Kamaruddin and R. B. Mydin, Effects of salivary pH on coating durability of two different aesthetic archwire coatings under a simulated intraoral environment, Saudi Dent. J., 32 (2020) 306–313. https://doi.org/10.1016/j.sdentj.2019.09.010

[2] M. K. Eltayeb, Y. E. Ibrahim, I. A. El Karim and N. M. Sanhouri, Distribution of white spot lesions among orthodontic patients attending teaching institutes in Khartoum, BMC Oral Health, 17 (2017) 88. https://doi.org/10.1186/s12903-017-0380-7.

[3] N. Sagarika, S. Suchindran, S. Loganathan and V. Gopikrishna, Prevalence of white spot lesion in a section of Indian population undergoing fixed orthodontic treatment: An in vivo assessment using the visual International Caries Detection and Assessment System II criteria J. Conserv. Dent., 15 (2012) 104-108. https://doi.org/10.4103/0972-0707.94572.

[4] A. Lucchese and E. Gherlone, Prevalence of white-spot lesions before and during orthodontic treatment with fixed appliances, Eur. J. Orthod., 35 (2013) 664-668. https://doi.org/10.1093/ejo/cjs070.

[5] Z. M. Al-Fadhily and M. A. Abdul-Hadi, Novel Coating of Orthodontic Archwires with Chlorhexidine Hexametaphosphate Nanoparticles, Int. J. Biomater., (2023) 9981603. https://doi.org/10.1155/2023/9981603.

[6] I. Chen, J. Chung, R. Vella, C. M. Weinstock, Y. Zhou and A.H. Jheon, Alterations in subgingival microbiota during full-fixed appliance orthodontic treatment-A prospective study, Orthod. Craniofac. Res., 25 (2022) 260-268. https://doi.org/10.1111/ocr.12534.

[7] H. H. Goh and B. Doubleday, Aids for mechanical cleaning of teeth with fixed braces, Cochrane Database of Systematic Reviews, 1 (2018). https://doi.org/10.1002/14651858.CD012931.

[8] J. A. Cury and L. M. Tenuta, Evidence-based recommendation on toothpaste use, Braz. Oral Res., 28 (2014) 1-7. https://doi.org/10.1590/S1806-83242014.50000001.

[9] T. S. Al-Jewair TS, S. Suri and B. D. Tompson, Predictors of adolescent compliance with oral hygiene instructions during two-arch multibracket fixed orthodontic treatment, Angle Orthod., 81 (2011) 525-531. https://doi.org/10.2319/092010-547.1.

[10] J. Song, H. Liu, M. Lei, H. Tan, Z. Chen, A. Antoshin, G. F. Payne, X. Qu and C., Redox-Channeling Polydopamine-Ferrocene (PDA-Fc) Coating to Confer Context-Dependent and Photothermal Antimicrobial Activities, ACS Appl. Mater. Interfaces., 12 (2020) 8915-8928. https://doi.org/10.1021/acsami.9b22339.

[11] D. Mitra, E. T. Kang and K. G. Neoh, Antimicrobial Copper-Based Materials and Coatings: Potential Multifaceted Biomedical Applications, ACS Appl. Mater. Interfaces., 12 (2020) 21159-21182. https://doi.org/10.1021/acsami.9b17815.

[12] S. Zhang, L. Wang, X. Liang, J. Vorstius, R. Keatch, G. Corner, G. Nabi, F. Davidson G.M. Gadd and Q. Zhao, Enhanced Antibacterial and Antiadhesive Activities of Silver-PTFE Nanocomposite Coating for Urinary Catheters, ACS Biomater. Sci. Eng., 5 (2019) 2804-2814. https://doi.org/10.1021/acsbiomaterials.9b00071.

[13] A. Panáček, L. Kvítek, M. Smékalová, R. Večeřová, M. Kolář, M. Röderová, F. Dyčka, M. Šebela, R. Prucek, O. Tomanec and R. Zbořil, Bacterial resistance to silver nanoparticles and how to overcome it, Nat. Nanotechnol., 13 (2018) 65-71. https://doi.org/10.1038/s41565-017-0013-y.

[14] H. A. Alaloosi, F. T. M. Noori, and A. K. Jidran, The Fundamental of Reduced Graphene Oxide with Nanosilver Composite Films Using the Spin Coating Technique, Eng. Technol. J., 40 (2022) 1023- 1028. http://doi.org/10.30684/etj.v40i8.2205.

[15] R. H. Abbasa, A. M. Haleem and A. K. Judran, Fabrication of Silver Nanoparticles in Aqueous Solution by Laser Technique and Study of Their Hemocompatibility and Antibacterial Effects Against Dental Decay Bacteria, Eng. Technol. J., 41 (2023) 543-552. http://doi.org/10.30684/etj.2023.136922.1329.

[16] Tabatabaei, F. S., Torres, R. and Tayebi, L. Biomedical Materials in Dentistry: Applications of Biomedical Engineering in Dentistry; Springer, 2020. https://doi.org/10.1007/978-3-030-21583-5_2.

[17] J. Siegel, M. Polívková, N. S. Kasálková, Z. Kolská and V. Svorčík, Properties of silver nanostructure-coated PTFE and its biocompatibility, Nanoscale Res. Lett., 8 (2013) 388. https://doi.org/10.1186/1556-276X-8-388.

[18] H. Qian, M. Li, Z. Li, Y. Lou, L. Huang, D. Zhang, D. Xu, C. Du, L. Lu and J. Gao, Mussel-inspired superhydrophobic surfaces with enhanced corrosion resistance and dual-action antibacterial properties, Mater. Sci. Eng. C Mater. Biol. Appl., 80 (2017) 566-577. https://doi.org/10.1016/j.msec.2017.07.002.

[19] T. Kameda, H. Sato, S. Oka, A. Miyazaki, K. Ohkuma and K. Terada, Low temperature polytetrafluoroethylene (PTFE) coating improves the appearance of orthodontic wires without changing their mechanical properties, Dent. Mater. J., 39 (2020) 721-734. https://doi.org/10.4012/dmj.2019-227.

[20] W. S. Hussain, J. K. Oleiwi and Q. A. Hamad, Study of Physical Properties of Biocomposite Based on the Polymer Blends Used for Denture Base Applications, Eng. Technol. J., 41 (2023) 1474 – 1487. http://doi.org/10.30684/etj.2023.141437.1496.

[21] M. Buerkle and Y. Asai, Thermal conductance of Teflon and Polyethylene: Insight from an atomistic, single-molecule level, Sci. Rep., 7 (2017) 41898. https://doi.org/10.1038/srep41898.

[22] V. Satulu, B. Mitu, V. Ion, V. Marascu, E. Matei, C. Stancu, and G. Dinescu, Combining Fluorinated Polymers with Ag Nanoparticles as a Route to Enhance Optical Properties of Composite Materials, Polymers (Basel), 12 (2020) 1640. https://doi.org/10.3390/polym12081640.

[23] V. Satulu, B. Mitu, A. M. Pandele, S. I. Voicu, L. Kravets and G. Dinescu, Composite polyethylene terephthalate track membranes with thin teflon-like layers: Preparation and surface properties, Appl. Surf. Sci., 476 (2019) 452-459. https://doi.org/10.1016/j.apsusc.2019.01.109.

[24] Y. Zhang, Q. Wang, C.S. Ramachandran, P. Guo and A. Wang, Microstructure and Performance of High-Velocity Oxygen-Fuel Coupled Physical Vapor Deposition (HVOF-PVD) Duplex Protective Coatings: A Review, Coatings, 12 (2022) 1395. https://doi.org/10.3390/coatings12101395.

[25] S. A. Mohammed, A. B. Mahmood and I. I. Al-Sheakli, Measurement of Surface Roughness of Copper Nickel Titanium Arch Wires at Dry and Wet Conditions: An In vitro Study, J. Res. Med. Dent. Sci., 7 (2019) 21-26.

[26] F. J. Gil, E. Espinar-Escalona, N. Clusellas, J. Fernandez-Bozal, M. Artes-Ribas and A. Puigdollers, New Bactericide Orthodonthic Archwire: NiTi with Silver Nanoparticles, Metals, 10 (2020) 702. https://doi.org/10.3390/met10060702.

[27] S. A. Hassanzadeh-Tabrizi, Precise calculation of crystallite size of nanomaterials: A review, J. Alloys Compd., 968 (2023) 171914. https://doi.org/10.1016/j.jallcom.2023.171914.

[28] Goetz-Neunhoeffer, F., and Hurle K. 2024. Mineralogical characterization of calcium phosphate cements for clinical needs, ed. J. M. Oliveira, R. L. Reis and S. Pina, pp. 199-217, Academic Press.

[29] H. A. Abdullah and R. A. Anaee, Characteristics and Morphological Studies of Nd Doped Titanium Thin Film Coating on SS 316L by DC Sputtering, Diyala J. Eng. Sci., 15 (2022) 22-30. https://doi.org/10.24237/djes.2022.15303.

[30] T. Siddiqui, M. K. Zia, M. Muaz, H. Ahsan and F. H. Khan, Synthesis and Characterization of Silver Nanoparticles (AgNPs) using Chemico-physical Methods, Ind. J. Chem. Anal., 6 (2023) 124-132. https://doi.org/10.20885/ijca.vol6.iss2.art4.

[31] I. Abiodun-Solanke, D. Ajayi and A. Arigbede, Nanotechnology and its application in dentistry, Ann. Med. Health Sci. Res., 4 (2014) 171-177. https://doi.org/10.4103/2141-9248.141951.

[32] J. Si, R. Ma, Y. Wu, Y. Dong and K. Yao, Microstructure and magnetic properties of novel powder cores composed of iron-based amorphous alloy and PTFE, J. Mater. Sci. 57 (2022) 8154–8166. https://doi.org/10.1007/s10853-022-07199-4.

[33] Y. M. Shulga, A. V. Melezhik, E. N. Kabachkov, F. O. Milovich, N. V. Lyskov, A. V. Irzhak, N. N. Dremova, G. L. Gutsev, A.Michtchenko, A.G. Tkachev and Y. Kumar, Characterisation and electrical conductivity of polytetrafluoroethylene/graphite nanoplatelets composite films, Appl. Phys. A 125, 460 (2019). https://doi.org/10.1007/s00339-019-2747-x.

[34] F. Li, M.D. Weir, J. Chen and H.H.K. Xu, Comparison of quaternary ammonium-containing with nano-silver-containing adhesive in antibacterial properties and cytotoxicity, Dent. Mater., 29 (2013) 450-461. https://doi.org/10.1016/j.dental.2013.01.012.

[35] A. Besinis, T. De Peralta T and R. D. Handy, Inhibition of biofilm formation and antibacterial properties of a silver nano-coating on human dentine, Nanotoxicology, 8 (2014) 745-54. https://doi.org/10.3109/17435390.2013.825343.

[36] D. M. Moreira, J. Oei, H. R. Rawls, J. Wagner, L. Chu, Y. Li, W. Zhang and K. Whang, A novel antimicrobial orthodontic band cement with in situ-generated silver nanoparticles, Angle Orthod., 85 (2015) 175-83. https://doi.org/10.2319/022314-127.1.

[37] S. Agnihotri, S. Mukherji and S. Mukherji, Immobilized silver nanoparticles enhance contact killing and show highest efficacy: elucidation of the mechanism of bactericidal action of silver, Nanoscale, 5 (2013) 7328-40. https://doi.org/10.1039/c3nr00024a.

[38] I. Francolini, C. Vuotto, A. Piozzi and G. Donelli, Antifouling and antimicrobial biomaterials: an overview, APMIS, 125 (2017) 392-417. https://doi.org/10.1111/apm.12675.

[39] G. Metin-Gürsoy, L. Taner and G. Akca, Nanosilver coated orthodontic brackets: in vivo antibacterial properties and ion release, Eur. J. Orthod., 39 (2017) 9-16. https://doi.org/10.1093/ejo/cjv097.

[40] S. Mei, H. Wang, W. Wang, L. Tong, H. Pan, C. Ruan, Q. Ma, M. Liu, H. Yang, L. Zhang, Y. Cheng, Y. Zhang, L. Zhao and, PK. Chu, Antibacterial effects and biocompatibility of titanium surfaces with graded silver incorporation in titania nanotubes, Biomater. 35 (2014) 4255-65. https://doi.org/10.1016/j.biomaterials.2014.02.005.

[41] N. F. N. N. A. Rahman, H. Hashim and S. I. Zubairi, Optimization of concentration and exposure time of polytetrafluoroethylene (PTFE) for the development of hydrophobic coating of drying chamber of spray dryer, IOP Conference Series: Earth and Environmental Science, 1200 (2023). https://doi.org/10.1088/1755-1315/1200/1/012044.

[42] S. P. Asrafali, T. Periyasamy, S. C. Kim and J. W. Lee, Enhanced wettability and adhesive property of ptfe through surface modification with fluorinated compounds, Mater. (Basel). 17 (2024) 3051. https://doi.org/10.3390/ma17133051.

[43] B. A. Aderibigbe, Metal-Based Nanoparticles for the Treatment of Infectious Diseases, Molecules, 22 (2017) 1370. https://doi.org/10.3390/molecules22081370.